Stochastic Modelling and Computational Sciences

GROWTH AND CONDUCTIVITY STUDIES IN TRIPOTASSIUM SODIUM MOLYBDATES SINGLE CRYSTAL

K. Bharath Raj
Assistant Professor of Physics, Girraj Government College(Autonomous), Nizamabad, India

ABSTRACT

The Aphthitalite crystals have the general formula $A_3C(BX_4)_2$, where A, C = Na, K and Rb and BX_4 tetrahedra are So_4, SeO_4, $(Cr)_4$, MoO_4 and WO_4. The crystal Tripotassium sodium molybdate ($K_3Na(MoO_4)_2$ was chosen and studied for Electrical properties like conductivity at various temperatures along the crystallographic axes.

Ferroelastic crystals have potential applications in electromodulators, ferroelastic gratings and many others. Slow evaporation technique at constant temperature was used to grow large single crystal. The investigation to be done along the crystallographic axes of these crystals has to identify all newly possible phase transitions. The electrical studies of the grown crystals are to be analyzed. The electrical conductivity and resistivity mechanisms are to be studied. Frequency dependent conductivity compared and analyzed. Complex impedance analysis, thermigravimetric analysis for the grown crystals studied further.

Keywords: Ferroelastic crystals, Electrical conductivity, Resistivity, Phase transition.

1. INTRODUCTION

The $K_3Na(MoO_4)_2$ or KNMo crystal, which frequently displays ferroic phases, is a member of the chemical family such as $A_3C(BX_4)_2$ (here A, C = Li, Na, K, Rb, Cs, NH_4, & BX_4 = SO_2, SeO_4, CrO_2). Trial reconnaissance for the resources show that $K_3Na(MoO_4)_2$, $K_3Na(CrO_4)_2$ and $K_3Na(SeO_4)_2$ go through ferroelastic stage changes on an origin bunch $\bar{3}$ ml to 2 lm at around 513 K, 239 K and at 346 K, individually [1]. At 853 K, Furthermore, at these continuous the order of second transition on 239 K, KNMo undergoes a second structural phase transition with a likely reduction in symmetry to 3 m from 6 lmmm [1]. The ferroelastic stage progress of KNMo is coupled by efforts for two crystallographic ally free K^+ positive ion, as well as by shift and shifting of $[MoO_4]^2$[4]. Mroz et al. [11] Developed a Landau model to present a qualitative explanation on ferro elastic transition and carried out studies using Brillonin scattering. Electron paramagnetic reverberation study [6] proposes the presence of a disproportionate stage. From acoustical inspections [3], irregularities occurred retrieved similar for ferroelastic stage progress. The gem structure KNMo was concentrated by Madariaga et al. The crystal's cell dimensions are a = 6.156 (6) A^0 and c = 15.520 (2) A^0 when it is in its room temperature phase, according to [10]. The thickness of the precious stone is 2.97(2)gcm^{-3}. Therefore purpose is work out of MoO_2 tetrahedra, NaO6 octahedra and two distinct K(1)0_{10} and K(2))0_{12} mere muddled polyhedral assembled by the c-pivot. The softening place of the precious stone is 1160 K [2]. The Na-O distances in the NaO_6 octahedra are balance limited to a solitary worth of 2.364 A^0. The mean distances in the K(1) O_{10} and O_{12} polyhedra are 2.969 A^0 and 3.15 A^0 separately. The distances between Mo and O range from 1.613 A^0 to 1.6439 A^0. The upsides of the two potential bond points O-Mo-O, in the MoO_2 bunch (110.310 and 108.630), show a tiny twisting as for the ideal tetrahedral setup. The primary exploration of the area temperature stage (P_3ml)[8] revealed for construction is isomorphous to $K_3Na(SO_4)_2$ [9]. Fabry et al. solved the structure of the parallel combination $K_3Na(SO_4)_2$ at both high and low temperatures. Al. [6] which due to high temperature shown the period of $K_3Na(SeO_4)_2$ is isomorphic on the heavy temperature of room at the periods of $K_3Na(SO_4)_2$ and $K_3Na(MoO_4)_2$.

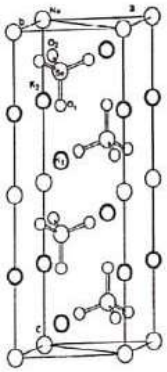

Figure 1.1 is a view of the trigonal phase of $K_3Na(MoO_4)_2$ single crystal along the c-axis.

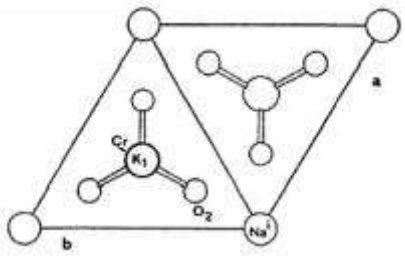

Figure 1.2 View along the c-axis of $K_3Na(MoO_4)_2$ crystal

Figure 1.1 shows the room temperature stage (three-sided) of $K_3Na(MoO_4)_2$ single valuable stone with two unit cells which are associated by the lattice understanding along the c-turn. Fig 1.2 is a point of view on the three-sided time of $K_3Na(MoO_4)_2$ single pearl along the c-center point. A truly complete study of the past examinations on KNaMo single jewel is positive. In this paper the outcomes of the electrical conductivity of KNaMo single valuable stone is presented.

2. Experimental setup

2.1 Experiment MODULATION

Single valuable stones of K3Na(MoO4)2 were created at consistent temperature of 310 K from splashed watery plans by languid dispersal technique. The blend's stock reagents were molybdic corrosive and synthetically pure sodium and potassium hydroxides. Three-crease recrystallization from refined water removed the union product. Over the course of 40 to 45 days, a marginally pink, highly formed gem with a maximum edge length of approximately 20 mm was obtained. Using the carefully programmed temperature regulator, both are kept at a constant temperature of 310 K and controlled to a precision of ±0.05 K. During the development, the precious stone was constantly turned in both clockwise and hostile to clockwise headings utilizing the gem pivot component.

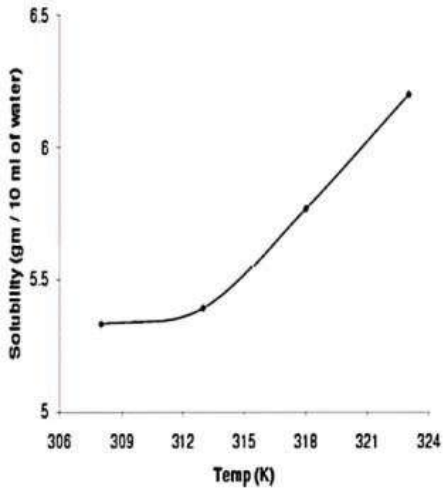

Figure 2.1: Solubility curve of $K_3Na\ (MoO_4)_2$

The $K_3Na(MoO_4)_2$ crystal's solubility was determined at various temperatures, and the solubility curve that can be seen in figure 2.1 was drawn.

2.2 Density Measurement

Using the Archimedes rule in carbon tetrachloride, an estimate of the precious stone's thickness was made. At room temperature, the developed example has a thickness of 2.96 gm/cm^3. This is very close to the detailed calculated value of 3.00 gm/cm^3.

2.3 Powder X-ray Diffraction of $K_3Na\ (MoO_4)_2$

The example powder is used for X beam research because the gem was well powdered. Using an X-beam diffractometer and Cu Ka(-1.542A^0) as the source, the X-beam powder diffraction was taken at a filtering rate of 20/min in the 2 territory 50-800. Figure 2.2 shows the XRD illustration of $K_3Na(MoO_4)_2$ valuable stone. The hkl planes have been recognized, and the outcomes are in great concurrence with the JCPDS [11] record. Table 2.1 provides the revealed and recognized hkl values. A contact goniometer is used to estimate the gem's interfacial points. By knowing the cross-segment limits, valuable stone system and space pack one can fabricate a stereographic plot by using the PC program 'Jcrystal'. Table 2.2 depicts the processed and deliberate interfacial points.

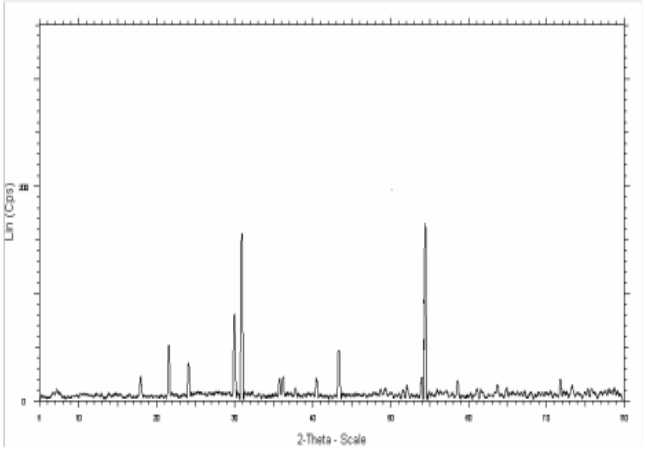

Figure 2.2: Room temperature XRD pattern of grown $K_3Na\ (MoO_4)_2$ crystals

values of Reported		Values of Identified	
d	hkl	d	hkl
5.0723	100	4.9637	100
4.2053	101	4.1407	101
3.7605	002	3.6879	002
3.0208	102	2.9721	102
2.9285	110	2.8830	110
2.5070	003	2.47/7	003
2.2474	103	2.2458	103
2.1026	002	2.0949	002
1.7829	023	1.7683	023
1.7080	212	1.6764	212
1.6507	300	1.6852	300
1.5822	114	1.5538	114
1.4642	220	1.4581	220
1.3380	115	1.3153	115

Table 2.1: Comparison of reported and identified hkl values of $K_3Na(MoO_4)_2$ single crystal

Crystal faces		Interfacial angle between	
Face1	Face2	Computed value	Measured
001	010	90.00	89.99
001	100	90.00	89.99
001	-110	90.00	89.99
001	-100	90.00	89.99
010	100	59.871	59.99
010	-110	60.06	59.99
010	-100	120.13	120.00
100	-100	180.00	180.00
-100	-110	60.06	60.00

Table 2.2: Interfacial angles of $K_3Na(MoO_4)_2$ single crystal measured & compared

3. Measurements of DC Conductivity

A conductivity cell was used to mount the prearranged example. The temperature circulator shower kept the entire cell cool. The temperature of the shower and in this method of the model was varied in propels. The speed of temperature expanded as 0.5 K/min. A programmable electrometer was used to estimate the DC conductivity. Current through the model was noted by applying a voltage of 10 V. For both the warming run and the cooling run, estimates were transmitted along an and c-tomahawks in the temperature range of 300 K to 410 K.

3.1 DC Conductivity along A-Axis

The DC electrical conductivity of $K_3Na(MoO_4)_2$ single crystal along a-axis was measured at different temperatures and the plot of temperature versus conductivity is shown in figure 3.1 and figure 3.2.

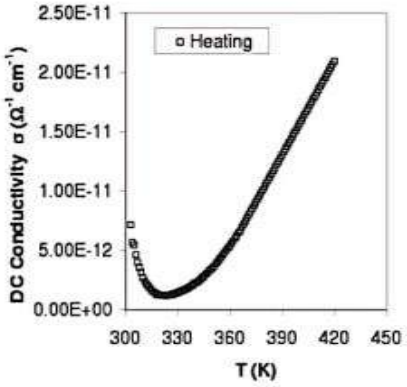

Figure 3.1: Variation of DC conductivity with temperature along a-axis in heating cycle

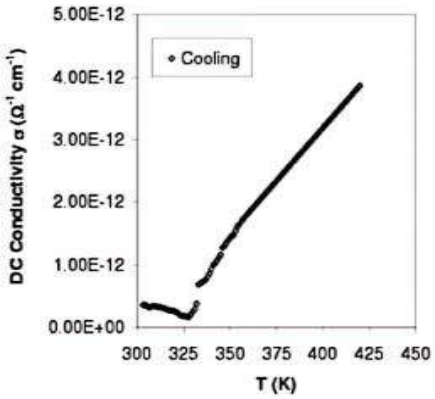

Figure 3.2 : Variation of DC conductivity with temperature along a-axis in cooling cycle

The temperature versus conductivity in the warming and cooling cycle shows an oddity at around 325 K demonstrative of conductivity least in the temperature range considered. After 325 K, the conductivity increases rapidly and linearly with temperature. The worth of conductivity is 1.4 x 10-11Ω^{-1}cm-^{1} for warming cycle and 3.55 x 10^{-}13Ω^{-1}cm-^{1} for cooling cycle at 305 K.

3.1 DC Conductivity

The DC electrical conductivity of $K_3Na(MoO_4)_2$ single precious stone along a-hub was estimated at various temperatures and the plot of temperature versus conductivity is displayed in figure 3.1 and figure 3.2.

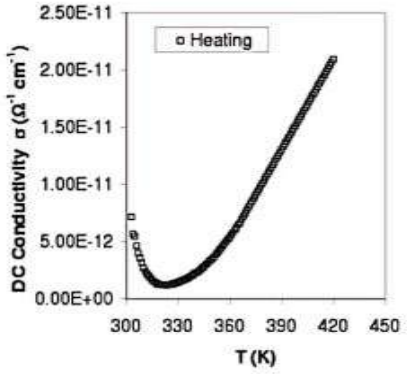

Figure 3.1: Variation of DC conductivity with temperature along a-axis in heating cycle

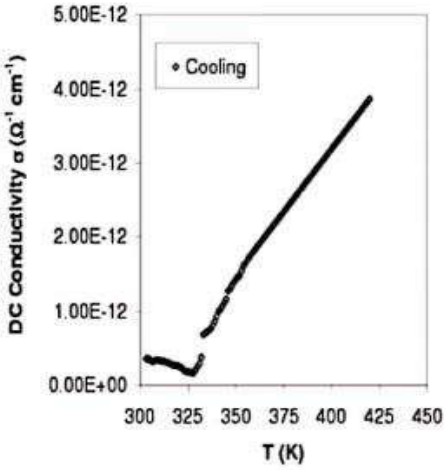

Figure 3.2: Variation of DC conductivity with temperature along a-axis in cooling cycle

The temperature versus conductivity in the warming and cooling cycle shows an oddity at around 325 K demonstrative of conductivity least in the temperature range considered. After 325 K, the conductivity increases rapidly and linearly with temperature. The worth of conductivity is 1.4 x 10-11Ω^{-1}cm-^{1} for warming cycle and 3.55 x 10-13Ω^{-1}cm-^{1}for cooling cycle at 305 K.

3.2 DC Conductivity along C-Pivot

The dc electrical conductivity studies in the $K_3Mo(CrO_4)_2$ Single crystal along the c-axis during the heating and cooling cycles are depicted in Figures 3.3 and 3.4, respectively.

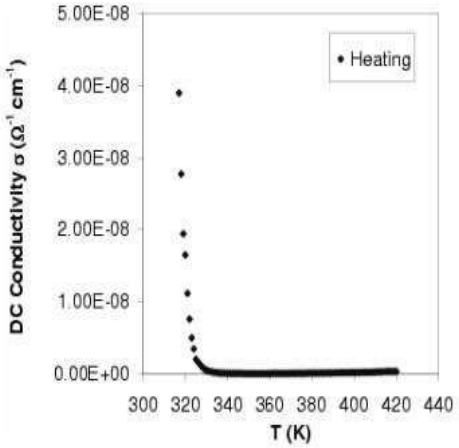

Figure 3.3: Variation of DC conductivity with temperature along c-axis in heating cycle

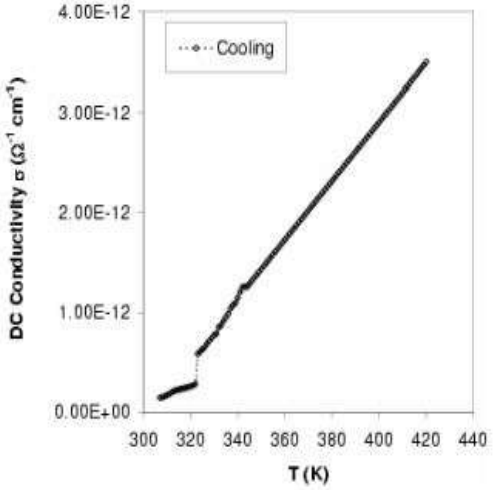

Figure 3.4: Variation of DC conductivity with temperature along c-axis in cooling cycle

The conductivity peculiarity in the warming cycle is seen at around 326 K yet in the cooling cycle the irregularity is seen at around 325 K appearance a warm hysteresis of 3 K. The worth of conductivity is 1.65 x 10 - 8 $\Omega^{-1}cm^{-1}$ and 6.49 x 1013 $\Omega^{-1}cm^{-1}$ for warming and cooling cycle at 326K individually. 3.3 Initiation energy along an and c tomahawks The actuation energies of the $K_3Na(MoO_4)_2$ single gem can be tracked down utilizing the plot of 1000/T versus log of conductivity, which can be addressed by the Arhenius connection.

$\sigma = \sigma_0 \exp(- E/kgT)$

where σ_0 is the pre-remarkable component, E is the actuation energy, kg is the Boltzman's steady and T is the outright temperature. The slope of the 1000/T vs. ln plot is used to calculate the activation energies. The enactment energies in the warming and cooling run for an and c tomahawks is shows in the table 3.1

Axis	Activation energy in eV	
	Heating	Cooling
A	0.369	0.302
C	0.262	0.281

Table 3.1: Activation energies along a and c axes.

The pre-exponential factor σ_0 is calculated from the 1000/T Vs ln σ plot after applying linear regression and extrapolation to the ln σ axis, σ_0 is the characteristic of each material. The pre- exponential factor σ_0 is the conductivity value when T tends to infinity. The value for σ_0 for a-axis is 2.367 x 10^{-9} $\Omega^{-1}cm^{-1}$ and for c-axis is 2.707 x 10^{-9} $\Omega^{-1}cm^{-1}$

4. AC Conductivity

For the first time, the $K_3Mo(CrO_4)_2$ single crystal is the subject of AC electrical conductivity and dielectric studies. Dielectric studies show the reaction of the material to an electric field. The bulk capacitance, resistance, and relaxation time for the a and c axes are obtained through complex impedance analysis. In this part the air conditioner conductivity spectra estimated along an and c tomahawks in the temperature range 305 K - 440 K for a few frequencies are accounted for.

4.1 Evaluation of Conductivity

AC conductivity on repeat can be conveyed by the going with condition "complete()" rises to " $\sigma_{total}(\omega) = \sigma(0) + A\omega^{r}$" This condition is known as Jonscher's Comprehensive Power Guideline condition where An is the pre sensational variable and r is the repeat type which is overall not precisely or identical to one [14]. Figure 4.4 and

4.5 show the repeat dependence of assessed AC electrical conductivity for an and c hatchets at different temperatures.

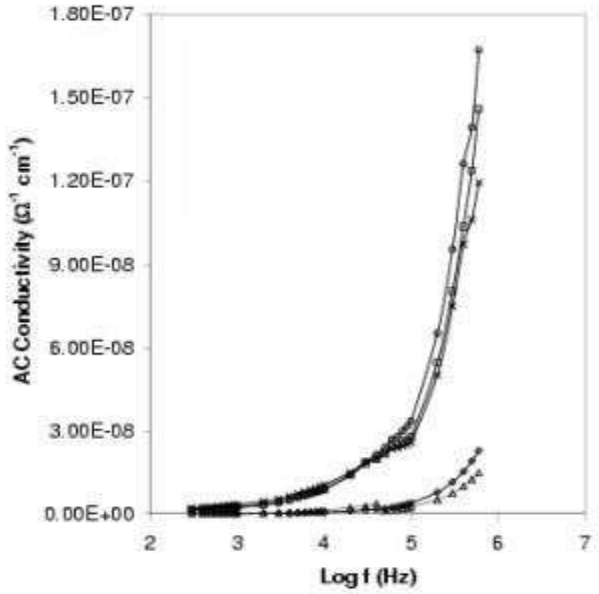

Figure 4.4 Variation of measured AC conductivity with frequency along a-axis.

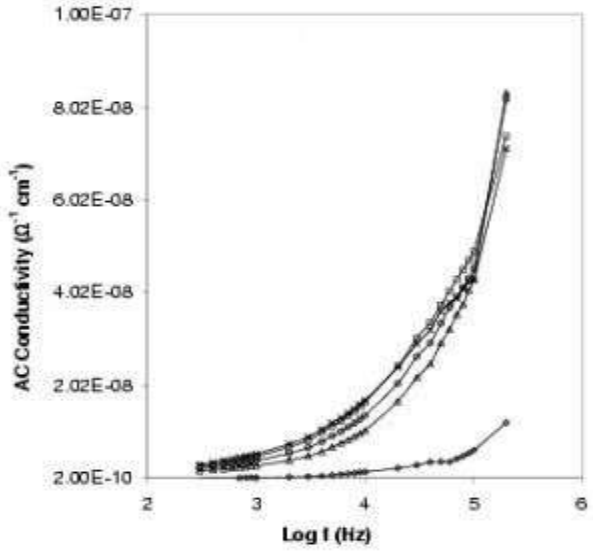

Figure 4.5 Variation of measured AC conductivity with frequency along c-axis.

It is clear from the chart that the deliberate AC electrical conductivity is a capability that increments for the two tomahawks. The commitment due to unadulterated AC conductivity is observable at lower frequencies and higher temperatures, where the deliberate AC conductivity is slightly higher than the DC conductivity. At higher frequencies and higher temperatures, the responsibility of pure AC conductivity to the outright conductivity is more, through the responsibility of DC conductivity can't be overlooked. At higher frequencies and lower temperatures, pure ac conductivity obligation to amount to ac conductivity thoroughly beats that in view of DC conductivity. At lower frequencies the probability of between well bobbing beats that due to intra-well bouncing and complete conductivity generally comparable to the dc conductivity [14]. With increasing signal frequency

comes an increase in the likelihood of intra-well hopping, and pure ac conductivity significantly raises total conductivity. The value of r' in the above condition is the inclination of the plot of ln σ_{ac} against ln ω (ω = 2πf). The incline of the plot of "total against"r can be used to separate the dc conductivity from the overall conductivity and the pre-significant element. The forced air system conductivity can be speculatively resolved using the above values, by the power guideline limits in the Boundless Power Guideline condition. The speculatively fitted curve is almost same as that of the exploratory characteristics. The surveyed power guideline limits a given in tables 4.3 and 4.4.

Temperature(K)	$\sigma(\theta)(\Omega^{-1}cm^{-1})$	r	A
305	2.75×10^{-11}	0.76946	1.2494×10^{-11}
325	1.56×10^{-12}	0.5802	1.1291×10^{-12}
365	4.4×10^{-10}	0.6425	6.5862×10^{-12}
385	7.0×10^{-10}	0.6096	4.2599×10^{-11}
405	1.0×10^{-9}	0.5543	1.6975×10^{-11}

Table 4.3: Power law Parameters of $K_3Na(MoO_4)_2$ for different temperatures along a-axis.

Temperature(K)	$\sigma(\theta)(\Omega^{-1}cm^{-1})$	r	A
305	1.5×10^{-12}	0.7239	5.5454×10^{-13}
325	9.0×10^{-10}	0.6853	4.5931×10^{-12}
365	1.0×10^{-9}	0.6227	1.134×10^{-13}
385	1.5×10^{-9}	0.6245	1.1927×10^{-11}
405	1.6×10^{-9}	0.5670	2.2875×10^{-11}

Table 4.4: Power law Parameters of $K_3Na(MoO_4)_2$ for different temperatures along c-axis.

Obviously σ(θ), r and A are temperature subordinate amounts. For the a-axis, the value r is between 0.77 and 0.55, while for the c-axis, it is between 0.72 and 0.57. Hypothetical fitting was noticed.

Temperature subordinate conductivity spectra Temperature subordinate ac conductivity can be determined utilizing the connection given underneath.

$\sigma = \varepsilon_0 \omega \varepsilon''$

where is the dielectric loss, f is the angular frequency, and 0 is the static dielectric constant. The genuine piece of the perplexing conductivity taken at 1, 5 and 10 KHz along the a and c axis of $K_3Na(MoO_4)_2$ single gem in the temperature range 305 K - 440 K are displayed in figure 4.6 and 4.7 separately.

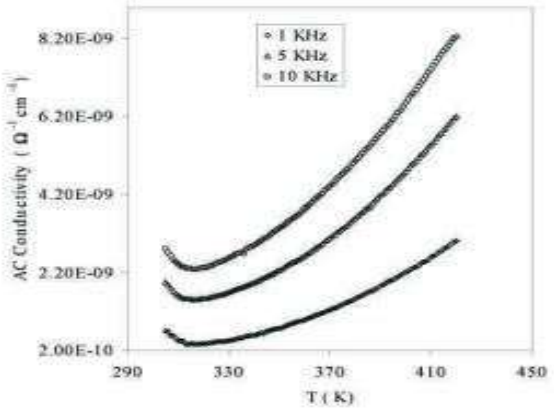

Figure 4.6: Variation of measured AC conductivity with temperature along a-axis

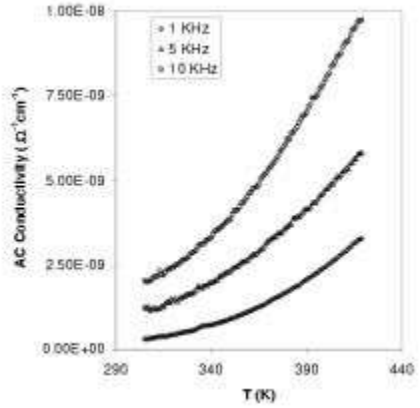

Figure 4.7: Variation of measured AC conductivity with temperature along c-axis

The worth of conductivity emphatically relies upon recurrence. Along a-hub the air conditioner conductivity irregularity was seen at around 326 K for all frequencies. For c-pivot the peculiarity was not plainly noticed. The temperature reliance of ac conductivity is normally given by the Arhenius condition.

$\sigma = \sigma_0 \exp(-E/KBT)$

From the plot of 1000/T Versus ln σ, the enactment energies can be found out. The acquired qualities are classified in the table 4.5 displayed underneath.

Axis	Activation energy in eV		
	1 KHz	3 KHz	10 KHz
a	0.2522	0.1652	0.15
c	0.2374	0.1652	0.16

Table 4.5: Activation energy values obtained for $K_3Na(CrO_3)_2$

The actuation energy is found to diminish at higher recurrence. This element is reliable with the Jonscher's investigation of ac conduction [18].

5 DISCUSSION

DC electrical conductivity studies of the $K_3Na(MoO_4)_2$ single crystal along its crystallographic axes exhibit conductivity anomaly at around 326 K. In the cooling run along c-axis this normally is shifted to 323 K, sharing a thermal hysteresis of about 3 K. After the transition region the conductivity seems to increase continuously with temperature. AC electrical conductivity studies also have a signature for the anomaly around 316 K. Temperature variation of dielectric constant along a-axis and variation of loss tangent with temperature gives the same information about the anomaly around 326 K. So the possibility of a phase transition around 326 K is highlighted. This anomaly is observed for the first time, in addition to the already reported phase transition for $K_3Na(MoO_4)_2$ at 239 K and 853 K. Thermo-gravimetric analysis of the sample crystal shows no mass reduction in the temperature ranges 305 K to 873 K. For thermo-gravimetric analysis, weight of the sample taken was 6.869 mg and the heating rate was maintained at 3^0C in nitrogen atmosphere. TGA curve (figure 5.1) shows that $K_3Na(MoO_4)_2$ crystal is stable in the entire temperature region studied. The melting point of the crystal is reported to be at 1160 K. So the observed anomaly can be attributed as a new phase transition.

From the models impedance investigation of $K_3Na(MoO_4)_2$ single gem it was found that low recurrence spikes are gotten for specific temperatures because of terminal polarization. Conductivity follows Jonscher's universal power law, as evidenced by its frequency-dependent variation. Conductivity varies in a power law fashion in the high

frequency region, whereas it is independent of frequency in the low frequency region. It's obvious from the plot that over a specific point the conductivity increments straightly with recurrence.

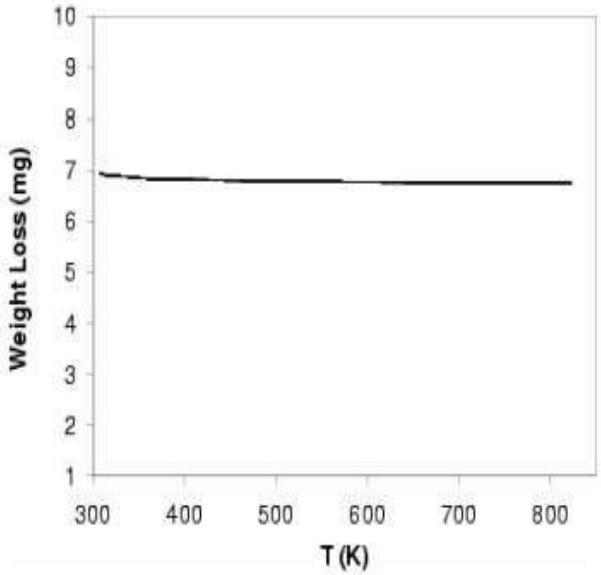

Figure 5.1: Thermogravimetric graph for the grown sample $K_3Na(MoO_4)_2$

It is likewise certain that the DC commitment is significant at low frequencies and high temperatures, whereas the recurrence subordinate tem overwhelms at high frequencies. The recurrence type boundary and DC conductivity are separated from these plots. Figures 5.2 and 5.3 show the comparison of the theoretically fitted curves using the power law parameters and the experimental curves for a and c axes respectively.

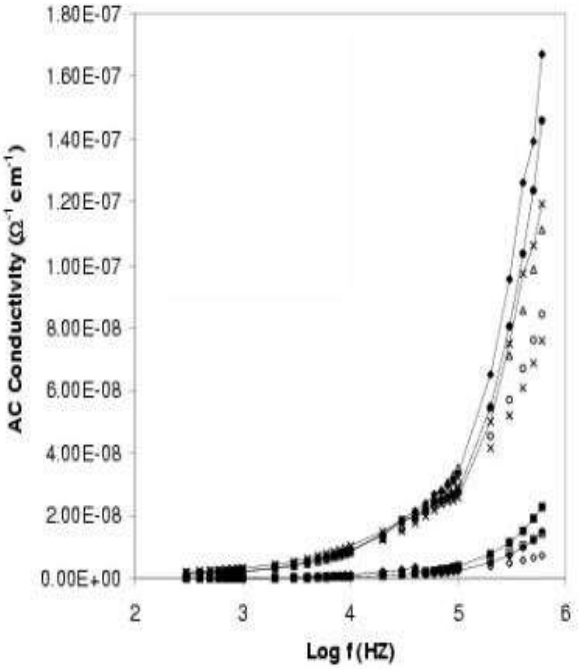

Figure 5.2: Comparison of theoretically fitted and experimental curves along a-axis.

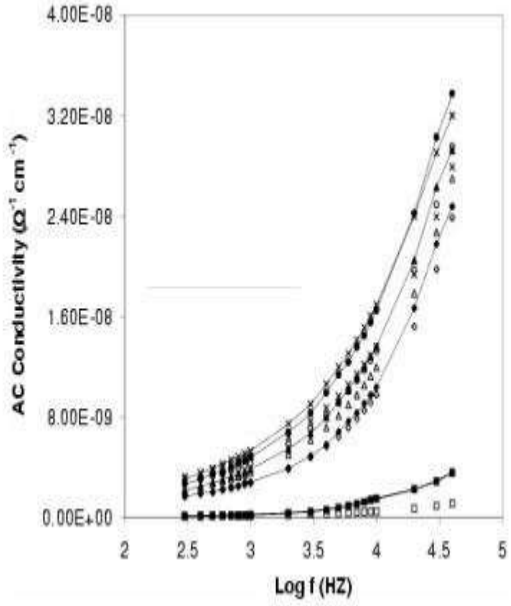

Figure 5.3: Comparison of theoretically fitted and experimental curves along c-axis.

The theoretically fitted and experimental curves are in fairly good agreement in the low frequency region but slight differences were observed in the high frequencies region.

The activation energies were calculated for both DC and AC conductivities which show a decreasing trend with increasing frequency.

6. CONCLUSION

Large single crystals of $K_3Na(MoO_4)_2$ single crystal was grown by solution growth technique and its morphology was in very good agreement with computer generated morphology using the computer program 'Shape'. The identified hkl planes are in well agreement with the reported hkl values. Density of the grown crystal was determined and found reported to be matching with the reported values.

The conductivity and dielectric studies of $K_3Na(MoO_4)_2$ single crystal indicates a newly observed possible phase progress at around 326 K in the gem. DSC concentrates in a similar manner maintains this discernment. To understand how this stage progresses, further investigation is required. From the astounding impedance assessment, the ionic thought of conductivity is uncovered. The variation in conductivity with recurrence demonstrates that intra-well jumping takes precedence over between-well bouncing at lower frequencies, while intra-well jumping is more likely to occur at higher frequencies jumping increments.

REFERENCES

1. J. Fabry, V.Petricek, I. Cisarova, 1st August, 1997, chemistry, Acta crystallographica Section B-structural science.
2. Ferroelectric and Ferroelastic Phase Transitions in Molybdates and Tungstates of Monovalent and Bivalent Elements, V. A. Isupov, Ferroelectrics, Volume 322, 2005 - Issue 1
3. J. Fabry, T. Breczewski and G. Madariaga. Acta. Cryst, B 50, 13-22, (1994).
4. A.K. Radhahov, E.V. Charays, B. Morz, C. Tien, Z. Tylzynki, C.S. Wur, Physics of the Solid State, Vol 46, No4, 775 – 779, (2004).
5. Krajewski T, Morz B, Piskunowicz P and Breczewski. T. Ferroelectrics 106, 225, (1990).

6. Fabry J, Breczewski, T and Petricek, V, Acta Crystallogr. B. 49, 826, (1993).
7. S. Jerzak, J.Phys. Condens Matter, 15, 8725 – 8736, (2003).
8. T. Krajewski, P.Piskunowicz, B.Mroz, Phys, Status Solidi, (a) 135, 557, (1993).
9. Okada, K and Ossaka, J, Acta Crystallogr, B, B36, 919, (1980).
10. G. Madariaga andT. Breczewski, Acta, Cryst.C 46, 2091 – 2021, (1990).
11. B. Mroz, H. Kiefte, M.J.Clouter and J.A. Tuszynski, Phys, Rev B 43, number I, (1991).
12. Joint Committee for Powder Diffraction Studies (JCPDS) file no; 82 – 0536, (1994).
13. Gilberto T. Nitsu, Hirotoshi Nagata, Ana C.M. Rodrigues, Journal of Applied Physics, Volume 95, Number 6, March, (2004).
14. A.J.Bosman, H.A. Van Dal, Adv. Phys., 19, 77, (1970).
15. Affifi M A Belheet A EAbd.Elwahab F Aliya H F: Vacuum, 61, 9-17, (2001).
16. M. Sayer, A. Mansingh, J.B.Webb, J.Phys, C. Solid State Physics 11, 315, (1978).
17. HartmannE: Cry. Res. Tech. 36, 911 – 916, (2001).
18. Bhattacharys S, Saha SK Chakrovarthy M, Mandal B M, Chakarvorthy D, Goswami K: J. Pol. Sci. Poly Phys.,19, 77, (1970).
19. Eichner, M. Kaczmarski, M. Wiesner, B. Mrox, Ferroelectric, 303, 31, (2004).
20. R.H. Chen, C.S. Shem, T. Fukami, Journal of Physics and Chemistry of Solids, 63, 203-212(2002).

.